PAPER

All-polymer methylammonium lead iodide perovskite microcavities†

Paola Lova, [ID] [a] Paolo Giusto,‡[a] Francesco Di Stasio, [ID] [a] Giovanni Manfredi,[a,b] Giuseppe M. Paternò, [ID] [b] Daniele Cortecchia, [ID] [c,d] Cesare Soci[c] and Davide Comoretto [ID] *[a,b]

Thanks to a high photoluminescence quantum yield, large charge carrier diffusion, and ease of processing from solution, perovskite materials are becoming increasingly interesting for flexible optoelectronic devices. However, their deposition requires wide range solvents that are incompatible with many other flexible and solution-processable materials, including polymers. Here, we show that methylammonium lead iodide ($MAPbI_3$) films can be directly synthesized on all-polymer microcavities *via* simple addition of a perfluorinated layer which protects the polymer photonic structure from the perovskite processing solvents. The new processing provides microcavities with a quality factor $Q = 155$, that is in agreement with calculations and the largest value reported so far for fully solution processed perovskite microcavities. Furthermore, the obtained microcavity shows strong spectral and angular redistribution of the the $MAPbI_3$ photoluminescence spectrum, which shows a 3.5 fold enhanced intensity with respect to the detuned reference. The opportunity to control and modify the emission of a $MAPbI_3$ film *via* a simple spun-cast polymer structure is of great interest in advanced optoelectronic applications requiring high colour purity or emission directionality.

Introduction

Nowadays, new and more efficient optoelectronic devices are being constantly developed thanks to the discovery and improvement of new materials. Such developments have allowed the fabrication of fully solution-processed devices, which enables low-cost and mechanically flexible applications. Photonic structures based on solution-processed polymers are among these novel devices.

Solution-processed multilayered structures can be fabricated employing commodity polymers and fabrication techniques such as spin-coating,[1–8] dip-coating,[9] self-assembly,[10,11] and coextrusion.[12] We have previously shown that solution-processed multilayered structures can control the lumine-

[a]*Dipartimento di Chimica e Chimica Industriale, Università di Genova, 16146 Genova, Italy*
[b]*Istituto Italiano di Tecnologia, Center for Nano Science and Technology, 20133 Milano, Italy*
[c]*Centre for Disruptive Photonic Technologies, TPI, SPMS, Nanyang Technological University, 21 Nanyang Link, Singapore 637371, Singapore*
[d]*Energy Research Institute @NTU (ERI@N), Nanyang Technological University, 50 Nanyang Drive, Singapore 6375532, Singapore*
†Electronic supplementary information (ESI) available: Additional optical data and full characterization of the reference sample. See DOI: 10.1039/c9nr01422e
‡Present Address: Max Planck Institute of Colloids and Interfaces, Department of Colloid Chemistry, Am Mühlenberg 1, 14476 Potsdam-Golm, Germany.
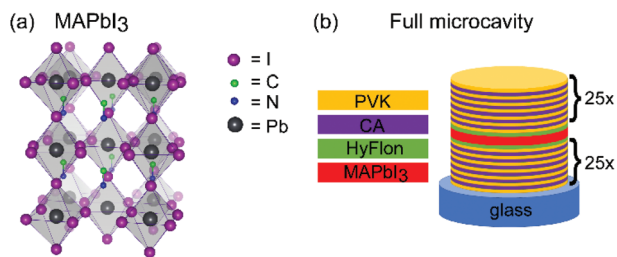
scence properties of emitters through directional redistribution of the oscillator strength,[5,6] and we have employed them to study light–matter interactions with both inorganic and hybrid emitters.[3,7,13] Given the ease of processing,[3] such architectures have also been successfully employed as efficient sensors,[14–18] lasers,[13,19,20] and all-optical modulators.[21] In general, solution-processed multilayered photonic structures have seen successful application in a variety of optoelectronic applications and their combination with perovskite[22,23] films is a natural development of their investigation. In fact, perovskites are very versatile semiconductors demonstrating a high photoluminescence quantum yield[24] that can be synthesized from solution as thin films,[25] colloidal nanocrystals[26,27] or 2D structures.[28,29] Among these systems, thin films of organo-lead halide perovskites of the general formula $APbX_3$ (Fig. 1a, where A = CH_3NH_3, or $CH(NH_2)_2$ and X = Cl, Br or I) have been successfully applied in solar cells,[25,29,30] light-emitting diodes,[31–33] where they demonstrated record efficiencies, and lasers.[22,34–36] Such materials are indeed increasingly studied thanks to the ease of tuning their optoelectronic properties and photoluminescence (PL) spectrum by varying their composition, for example changing the halide in their structure.[5,18] Unfortunately, perovskite thin films can only be cast from wide range solvents, that are solvents able to solubilize both polar and non-polar species. This makes them incompatible with polymers and reduces advantages related to solution pro-

Fig. 1 (a) Crystal structure of the MAPbI$_3$ perovskite thin film used in this study. (b) Scheme of the fabricated microcavity comprehending polymer layers of three different materials: PVK (poly(9-vinylcarbazole)), CA (cellulose acetate) and Hyflon® AD polymer.

cessing. Perovskite thin films have indeed been coupled with inorganic mesoporous photonic crystals,[37] and with self-assembled microsphere monolayers[38] but, to the best or our knowledge, coupling them with photonic structures available on a large area such as polymer multilayered distributed Bragg reflectors (DBRs)[3] is still challenging and it limits their application in lasing and light emitting devices.

In this work, we demonstrate a proof-of-concept fully solution processed microcavity fabricated using a methyl-ammonium lead iodide perovskite film (MAPbI$_3$, Fig. 1a) and all-polymer DBRs (Fig. 1b) achieving PL enhancement and its directional control. As previously discussed, the solution-processed perovskite film is synthesized employing a wide range solvent, which can dissolve any polymer structure during deposition. To overcome this issue, we fabricated a microcavity where the MAPbI$_3$ film is cast on a polymer DBR protected by a layer of a perfluorinated polymer. The protection layer prevents the perovskite precursor solvent from percolating through the polymer structure, thus dissolving it. A further polymer DBR was subsequently cast over the perovskite film to create a monolithic microcavity (Fig. 1b). The all-polymer DBRs were designed for partial spectral overlap between the photonic band gap (PBG) and the MAPbI$_3$ broad PL, thus allowing us to study the emission spectrum modifications. As a result, the PL spectrum of the MAPbI$_3$ film is strongly reorganized by the microcavity, as it induces spectral and angular redistribution of the emitted photons.

Experimental

Optical microcavity fabrication

The microcavity used in the study (Fig. 1b) was prepared by casting a toluene solution of poly(N-vinylcarbazole) (PVK, Across Organic, M_W = 135 600, n = 1.67)[39] (28 g L^{-1}; 3900 rpm) and a cellulose acetate (CA, M_r = 61 000, n = 1.46)[39] dissolved in diacetone alcohol (35 g L^{-1}; 4200 rpm) in an alternating sequence.[7,13] To form an optical microcavity with high reflectivity, the deposition of each layer was repeated 25 times. A perfluorinated Hyflon® AD polymer (Solvay Specialty Polymers, 35 g L^{-1}; 10 500 rpm) was cast as a capping layer, as described elsewhere.[17,40] The perfluorinated layer (Hy) strongly

hinders diffusion of the perovskite solvent (N,N-dimethyl-formamide, DMF) into the polymer stack, which would otherwise ruin the multilayer smoothness and periodicity. To improve adhesion of the perovskite, a thin layer of PVK cast from chlorobenzene (14 g L^{-1}; 10 500 rpm) was spun on top of the perfluorinated polymer. The perovskite thin film was prepared by reacting methyl ammonium iodide and lead acetate solution in DMF preheated at 100 °C and spin-casting it at 5000 rpm. Finally, the film was annealed at 80 °C for 15 minutes, before spin-casting a symmetric layered structure to complete the microcavity. A reference microcavity with blue-shifted PBG was prepared using the same procedure and decreasing the concentration of CA solution to 15 g L^{-1} to obtain thinner layers.

Perovskite thin film characterization

Perovskite thin films spun cast on glass were characterized by X-ray diffraction (XRD) using a Bruker D8 Advance with Bragg–Brentano geometry, Cu Kα radiation (λ = 1.54056 Å), a step increment of 0.02° and 1s of acquisition time. The surface topography of the perovskite film was measured using an Agilent 5500 Atomic Force Microscope operated in the acoustic mode. These measurements are reported in Fig. S1.†

Optical microcavity characterization and modelling

Reflectance and transmittance were measured with an optical-fiber setup coupled with a CCD spectrometer (Avantes AvaSpec-2048, 200–1150 nm, resolution 1.4 nm) and a deuterium–halogen Micropak DH2000BAL as a white light source. Photoluminescence and angle-dependent photoluminescence measurements have been recorded with a setup providing a solid angle of 0.002 steradian according to ref. 5, 7 and 21. The reflectance spectrum of the microcavity was modelled employing a transfer matrix method using previously reported refractive indexes as inputs (see Fig. S2†).[4,41,42]

Results and discussion

Fig. 2a displays the optical absorption and the PL spectra of a pristine MAPbI$_3$ thin film prepared on a glass substrate. The MAPbI$_3$ film on glass was prepared using the same procedure as for the microcavity emitting layer. The XRD pattern and the atomic force microscopy data reported in Fig. S1† confirm the formation of a MAPbI$_3$ film with a rugosity of 8 nm. As expected, the film shows a broad absorption in the visible spectral range extending over the whole visible spectrum, and a narrow PL (full-width-half-maximum, FWHM = 47 nm) centred at 756 nm. In Fig. 2b, we report the reflectance spectrum of the hybrid polymer/MAPbI$_3$ microcavity where a PBG between 753 and 875 nm is present.

A Fabry–Pérot pattern is clearly observed throughout the reflectance spectrum and it is caused by interference of the transmitted/reflected beams from the top and bottom surfaces of the polymer DBRs.[4] The homogeneity of the polymer DBRs is demonstrated by the reflectance spectra collected on
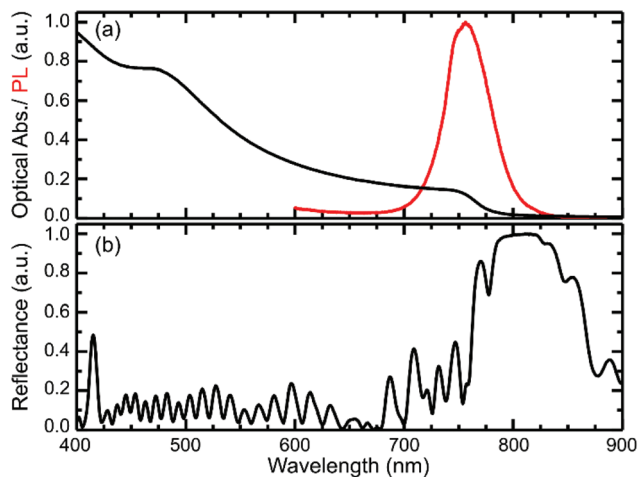
Fig. 2   (a) Optical absorption (solid black) and PL (solid red) spectra of a pristine MAPbI$_3$ film prepared on glass. (b) Representative reflectance spectrum of the hybrid polymer/MAPbI$_3$ microcavity.

different areas of the microcavity (Fig. S2†). In fact, only minor variations in the Fabry–Pérot pattern can be observed while the PBG spectral position and its FWHM are consistent throughout the measurement set.

Before proceeding with a more detailed discussion of the PL of the microcavity, a suitable reference must be identified. In our case, we have used a microcavity possessing a PBG detuned from the MAPbI$_3$ film PL spectrum (*i.e.* the PBG does not overlap the PL, Fig. S3†). Such a reference allows a direct comparison of the PL suppression/enhancement caused by the PBG without introducing spurious effects as, for example, variations in the light extraction efficiency caused by the different dielectric environments surrounding the MAPbI$_3$ film. The reference microcavity shows a PBG between 453 and 496 nm, thus it does not affect the PL of the emissive perovskite layer. Such a blue-shift of the PBG was obtained by reducing the thickness of the CA layer about six times, without further modification of the microcavity structure.

The PBG of the polymer DBRs strongly modifies the PL of the enclosed MAPbI$_3$ film compared to the pristine film prepared on glass. Fig. 3a shows the PL spectrum of the microcavity measured at a collection angle of 0° (*i.e.* perpendicular to the microcavity surface). First, the PL appears blue shifted due to the suppression of emission caused by the PBG from 784 nm upward. A sharp PL peak at 778 nm (corresponding to the microcavity reflection dip at the same wavelength, Fig. 3b) is observed, followed by other less intense ones at 763, 756 and 742 nm. Such peaks are assigned to the increased density of photonic states at the microcavity band edge that affect the perovskite emission spectrum similar to the cavity mode. The microcavity finesse ($Q = \lambda/\Delta\lambda$) can be evaluated from the FWHM of the peaks: FWHM = 5 nm and 8 nm for the 778 and the 763 nm PL peaks, respectively. We obtain values of $Q = 155$ and $Q = 95$ for the 778 and the 763 nm PL peaks, respectively, in full agreement with the calculation reported in Fig. S2.† These values are relatively high if one considers that the micro-
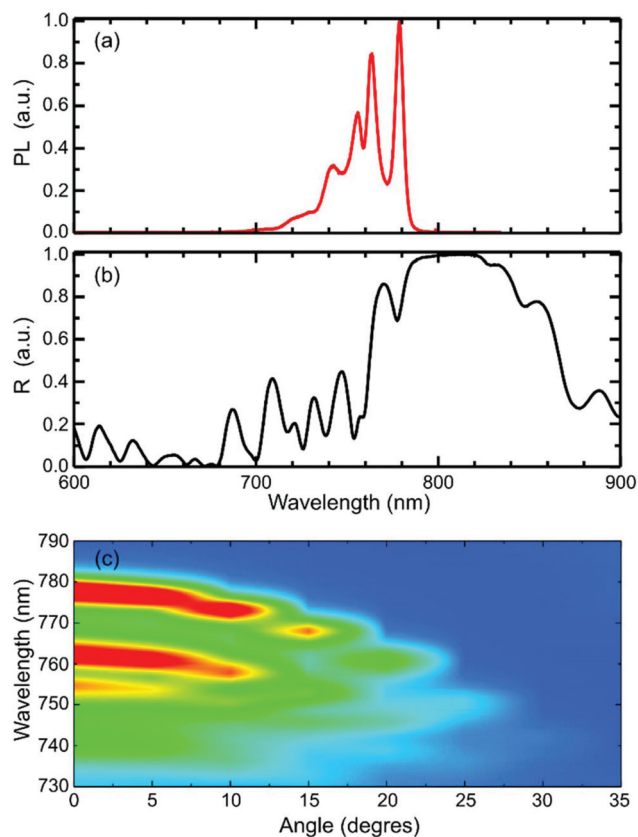

Fig. 3   (a) PL spectrum of the hybrid polymer/MAPbI$_3$ microcavity collected 0° (perpendicular to the microcavity surface). (b) Representative reflectance spectrum of the microcavity. (c) PL map *vs.* collection angle for the microcavity.

cavity constituent materials are polymers with refractive indexes $n = 1.67$ and $n = 1.46$ (for PVK and CA, respectively) which grant a reduced index contrast if compared to inorganic oxides.[2,3,43] Such finesse has been compared with the modelled data in Fig. S1.† The simulation shows that the obtained Q factor is consistent with a surface roughness of 0.3 nm for the PVK layers, 1 nm for the CA layers, and 8 nm for the MAPbI$_3$ defect layer (see Fig. S1 and S2† for details). The spectral position of the PL peaks depends upon the collection angle (Fig. 3c, Fig. S4 and S5†). The PL peaks follow the angular dispersion of the PBG, thus demonstrating that the observed modification is caused by the surrounding dielectric structure. The angular dispersion of the PBG is a well-known phenomenon in photonic structures possessing a periodical dielectric constant along only one direction (also known as 1D photonic crystals; transmittance spectra are reported in Fig. S4†). The PL peaks at 778 nm (0°) show a blue shift to 751 nm at 25° with the other peaks demonstrating an equal 27 nm shift.

Further evidence of the impact of PBG is the comparison with the reference sample. The same angle resolved PL measurements performed on the reference demonstrate only a monotonic decrease of the PL spectrum without further modifications (Fig. S4†). Importantly, the reference allows not only

evaluation of the spectral-shape modification but also variations in the emission intensity as well. Indeed, being the reference fully out-of-resonance from any photonic mode and carbazolyl moiety absorption,[44] it retains the same light extraction efficiency as the microcavity thus allowing for a more precise quantitative comparison of the spectral redistribution.[5,7] Fig. 4 compares the PL spectra of the microcavity and the reference at different collection angles. Fig. 4a–d shows that the

photonic band gap of the polymer dielectric DBRs not only suppresses the PL due to their high reflectance, but also enhances the cavity mode emission. This phenomenon is known as spectral redistribution of the PL oscillator strength and it is caused by a variation of the local density of photonic states within the microcavity.[3–5,7,45]

In general, the microcavity causes a PL enhancement ($PL_{cavity}/PL_{reference} > 1$) up to a collection angle of 20°, while
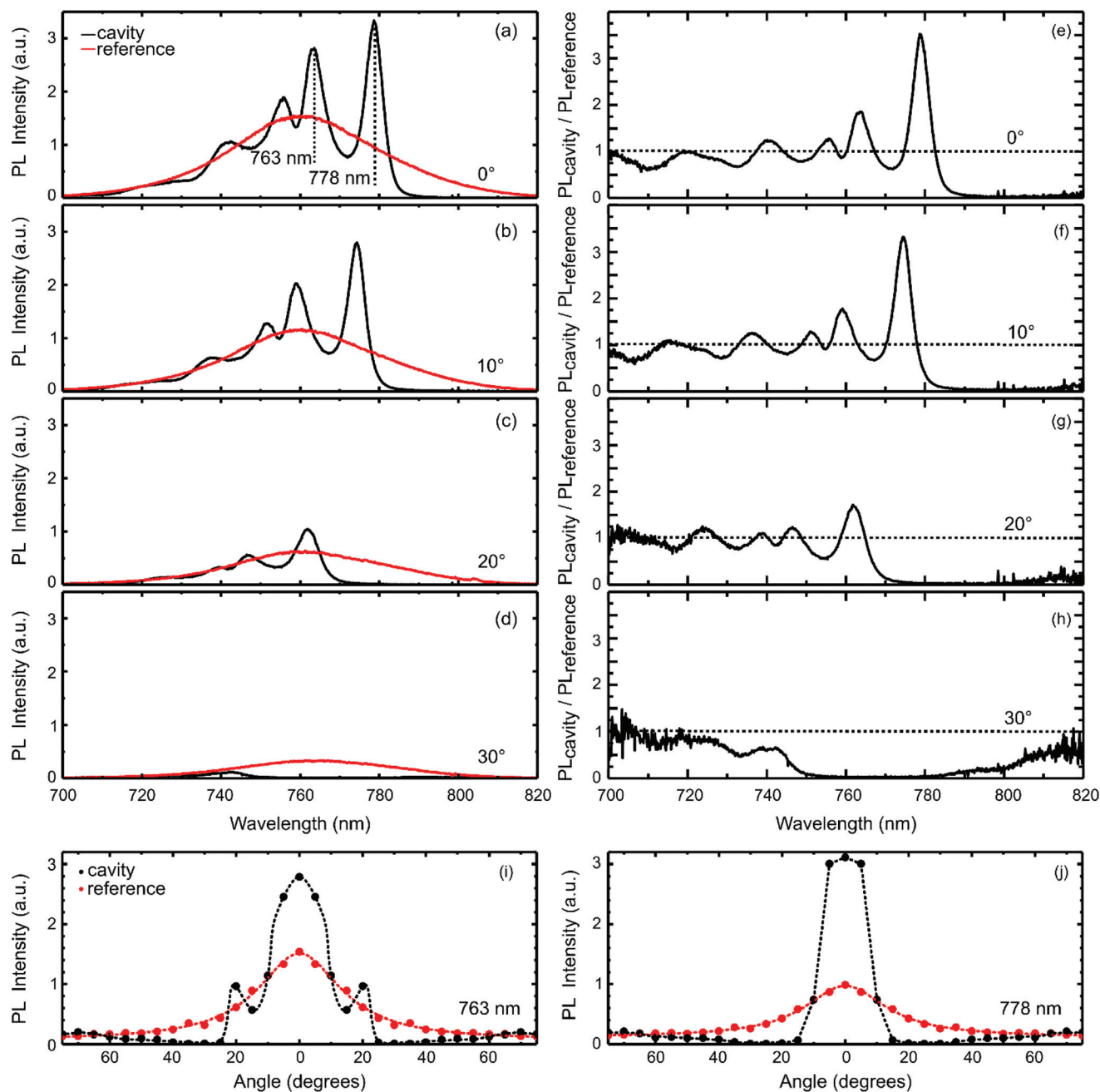

Fig. 4 (a–d) Comparison between the PL spectra of the microcavity (solid black curve) and the reference (solid red curve) at different collection angles. (e–h) Ratio of the PL between the microcavity and the reference ($PL_{cavity}/PL_{reference}$); a value above 1 indicates an enhancement while a value below 1 indicates suppression. Emission intensity at a fixed wavelength *vs.* detection angle for (i) 763 nm and (j) 778 nm for the microcavity (full black dots, wavelengths are highlighted in panel a) and for the reference (full red dots). The dashed fitting lines (same colour coding) are a guide to the eye.

above this angle, a PL suppression ($PL_{cavity}/PL_{reference} < 1$) is observed. The cavity mode observed in the reflectance spectra at 778 nm (0°) corresponds to a 3.5× enhancement of the PL intensity, while the second PL peak at 763 nm shows a 1.9× increase in intensity (Fig. 4e). In the wavelength range of 700–740 nm (*i.e.* where the PBG is not present), the $PL_{cavity}/PL_{reference} \approx 1$ as the PL spectrum is only modified by the interference fringes caused by the dielectric structure, thus demonstrating that the enhancement is caused by the cavity mode and the photonic band structure only.

Upon increasing the collection angle, the enhancement diminishes in intensity due to the increased overlap of the PBG with the perovskite PL. The angular and spectra redistribution caused by the polymer DBRs has an impact on the directionality of the PL. As previously discussed, the spectral redistribution of the PL oscillator strength gives rise to narrow emission peaks. In addition, the angular redistribution generated by the microcavity causes the PL peaks to blue shift upon increasing the collection angle. Therefore, at a fixed wavelength, the microcavity emission is highly directional combined with high colour purity (the latter induced by the narrow PL peak). To allow a clear observation of this phenomenon, in Fig. 4i and j, we present the PL intensity *vs.* angle for the two main emission peaks at 778 and 763 nm (Fig. 4a). The PL intensity shows a strong drop for collection angles above 20° (Fig. 4i and j). Interestingly, at 763 nm, an additional PL peak appears at 20° which is caused by the blue-shift of the emission peak observed at 778 nm (at 0°). Fig. 4i and j clearly show that the combination of the two redistribution phenomena not only gives rise to an enhancement of the emission at a fixed wavelength but also to a narrowing of the solid angle of emission. The latter effect is particularly useful, for example, in light-emitting diodes, where emission directionality can decrease optical losses, thus increasing the device efficiency.[46,47]

Conclusions

In conclusion, we have demonstrated for the first time the fabrication of monolithic microcavities based on $MAPbI_3$ and all-polymer DBRs despite the wide range solvents used for the synthesis of the perovskite film. The obtained microcavity shows a quality factor of 155, which is comparable with the state-of-the-art monolithic polymer microcavities and currently represents the highest reported for solution microcavities embedding perovskite thin films. The photonic structure causes a drastic modification of the $MAPbI_3$ film PL spectrum with the appearance of narrow emission peaks caused by the redistribution of the PL oscillator strength. The spectral redistribution combined with the angular dispersion caused by the DBRs PBG strongly reduce the emission angle at a fixed wavelength. These results show that all-polymer photonic structures are a viable tool for controlling the PL of a perovskite film *via* spectral and angular redistribution of the emitted photons. Therefore, such monolithic solution-processed microcavities are an ideal candidate for the fabrication, for example, of vertical-cavity-surface-emitting lasers exploiting the optical gain exhibited by perovskite materials.[36,48]

Conflicts of interest

There are no conflicts to declare.

Acknowledgements

References

1 D. Comoretto, *Organic and Hybrid Photonic Crystals*, Springer International Publishing, 1st edn, 2015.

2 S. Gazzo, G. Manfredi, R. Pötzsch, Q. Wei, M. Alloisio, B. Voit and D. Comoretto, *J. Polym. Sci., Part B: Polym. Phys.*, 2016, **54**, 73–80.

3 P. Lova, G. Manfredi and D. Comoretto, *Adv. Opt. Mater.*, 2018, **6**, 1800730.

4 L. Frezza, M. Patrini, M. Liscidini and D. Comoretto, *J. Phys. Chem. C*, 2011, **115**, 19939–19946.

5 P. Lova, V. Grande, G. Manfredi, M. Patrini, S. Herbst, F. Würthner and D. Comoretto, *Adv. Opt. Mater.*, 2017, **5**, 1700523.

6 P. Lova, D. Cortecchia, H. N. S. Krishnamoorthy, P. Giusto, C. Bastianini, A. Bruno, D. Comoretto and C. Soci, *ACS Photonics*, 2018, **5**, 867–874.

7 G. Manfredi, P. Lova, F. Di Stasio, R. Krahne and D. Comoretto, *ACS Photonics*, DOI: 10.1021/acsphotonics.7b00330. [Q4]

8 H. Míguez, S. M. Yang and G. A. Ozin, *Appl. Phys. Lett.*, 2002, **81**, 2493.

9 M. Faustini, D. R. Ceratti, B. Louis, M. Boudot, P.-A. Albouy, C. Boissière and D. Grosso, *ACS Appl. Mater. Interfaces*, 2014, **6**, 17102–17110.

10 Y. Wu, K. Zhang and B. Yang, *Adv. Opt. Mater.*, 2019, 1800980.

11 J.-H. Lee, C. Y. Koh, J. P. Singer, S.-J. Jeon, M. Maldovan, O. Stein and E. L. Thomas, *Adv. Mater.*, 2014, **26**, 532–569.

12 T. Kazmierczak, H. Song, A. Hiltner and E. Baer, *Macromol. Rapid Commun.*, 2007, **28**, 2210–2216.

13 G. Manfredi, P. Lova, F. Di Stasio, P. Rastogi, R. Krahne and D. Comoretto, *RSC Adv.*, DOI: 10.1039/c8ra01282b.

14 P. Lova, *Polymers*, 2018, 10.

15 W. Mönch, J. Dehnert, O. Prucker, J. Rühe and H. Zappe, *Appl. Opt.*, 2006, **45**, 4284–4290.

16 S. Gao, X. Tang, S. Langner, A. Osvet, C. Harreiß, M. K. S. Barr, E. Spiecker, J. Bachmann, C. J. Brabec and K. Forberich, *ACS Appl. Mater. Interfaces*, 2018, **10**, 36398–36406.

17 P. Giusto, P. Lova, G. Manfredi, S. Gazzo, P. Srinivasan, S. Radice and D. Comoretto, *ACS Omega*, 2018, **3**, 7517–7522.

18 P. Lova, C. Bastianini, P. Giusto, M. Patrini, P. Rizzo, G. Guerra, M. Iodice, C. Soci and D. Comoretto, *ACS Appl. Mater. Interfaces*, 2016, **8**, 31941–31950.

19 V. M. Menon, M. Luberto, N. V. Valappil and S. Chatterjee, *Opt. Express*, 2008, **16**, 19535–19540.

20 L. M. Goldenberg, V. Lisinetskii and S. Schrader, *Laser Phys. Lett.*, 2013, **10**, 55808.

21 R. J. Knarr, G. Manfredi, E. Martinelli, M. Pannocchia, D. Repetto, C. Mennucci, I. Solano, M. Canepa, F. Buatier de Mongeot, G. Galli and D. Comoretto, *Polymer*, 2016, **84**, 383–390.

22 B. R. Sutherland and E. H. Sargent, *Nat. Photonics*, 2016, **10**, 295–302.

23 S. D. Stranks and H. J. Snaith, *Nat. Nanotechnol.*, 2015, **10**, 391.

24 M. Abdi-Jalebi, Z. Andaji-Garmaroudi, S. Cacovich, C. Stavrakas, B. Philippe, J. M. Richter, M. Alsari, E. P. Booker, E. M. Hutter, A. J. Pearson, S. Lilliu, T. J. Savenije, H. Rensmo, G. Divitini, C. Ducati, R. H. Friend and S. D. Stranks, *Nature*, 2018, **555**, 497.

25 M. M. Lee, J. Teuscher, T. Miyasaka, T. N. Murakami and H. J. Snaith, *Science*, 2012, **338**, 643–647.

26 G. Rainò, G. Nedelcu, L. Protesescu, M. I. Bodnarchuk, M. V. Kovalenko, R. F. Mahrt and T. Stöferle, *ACS Nano*, 2016, **10**, 2485–2490.

27 Q. A. Akkerman, G. Rainò, M. V. Kovalenko and L. Manna, *Nat. Mater.*, DOI: 10.1038/s41563-018-0018-4.

28 L. Dou, A. B. Wong, Y. Yu, M. Lai, N. Kornienko, S. W. Eaton, A. Fu, C. G. Bischak, J. Ma, T. Ding, N. S. Ginsberg, L.-W. Wang, A. P. Alivisatos and P. Yang, *Science*, 2015, **349**, 1518–1521.

29 H. Tsai, W. Nie, J.-C. Blancon, C. C. Stoumpos, R. Asadpour, B. Harutyunyan, A. J. Neukirch, R. Verduzco, J. J. Crochet, S. Tretiak, L. Pedesseau, J. Even, M. A. Alam, G. Gupta, J. Lou, P. M. Ajayan, M. J. Bedzyk, M. G. Kanatzidis and A. D. Mohite, *Nature*, 2016, **536**, 312.

30 W. S. Yang, B.-W. Park, E. H. Jung, N. J. Jeon, Y. C. Kim, D. U. Lee, S. S. Shin, J. Seo, E. K. Kim, J. H. Noh and S. Il Seok, *Science*.

31 Z.-K. Tan, R. S. Moghaddam, M. L. Lai, P. Docampo, R. Higler, F. Deschler, M. Price, A. Sadhanala, L. M. Pazos, D. Credgington, F. Hanusch, T. Bein, H. J. Snaith and R. H. Friend, *Nat. Nanotechnol.*, 2014, **9**, 687–692.

32 X. Yang, X. Zhang, J. Deng, Z. Chu, Q. Jiang, J. Meng, P. Wang, L. Zhang, Z. Yin and J. You, *Nat. Commun.*, 2018, **9**, 570.

33 B. Zhao, S. Bai, V. Kim, R. Lamboll, R. Shivanna, F. Auras, J. M. Richter, L. Yang, L. Dai, M. Alsari, X.-J. She, L. Liang, J. Zhang, S. Lilliu, P. Gao, H. J. Snaith, J. Wang, N. C. Greenham, R. H. Friend and D. Di, *Nat. Photonics*, 2018, **12**, 783–789.

34 H. Zhu, Y. Fu, F. Meng, X. Wu, Z. Gong, Q. Ding, M. V. Gustafsson, M. T. Trinh, S. Jin and X.-Y. Zhu, *Nat. Mater.*, 2015, **14**, 636–642.

35 Q. A. Akkerman, M. Gandini, F. Di Stasio, P. Rastogi, F. Palazon, G. Bertoni, J. M. Ball, M. Prato, A. Petrozza and L. Manna, *Nat. Energy*, DOI: 10.1038/nenergy.2016.194.

36 Y. Jia, R. A. Kerner, A. J. Grede, B. P. Rand and N. C. Giebink, *Nat. Photonics*, 2017, **11**, 784–788.

37 W. Zhang, M. Anaya, G. Lozano, M. E. Calvo, M. B. Johnston, H. Míguez and H. J. Snaith, *Nano Lett.*, 2015, **15**, 1698–1702.

38 K. Meng, S. Gao, L. Wu, G. Wang, X. Liu, G. Chen, Z. Liu and G. Chen, *Nano Lett.*, 2016, **16**, 4166–4173.

39 L. Fornasari, F. Floris, M. Patrini, D. Comoretto and F. Marabelli, *Phys. Chem. Chem. Phys.*, 2016, **18**, 14086–14093.

40 WO/2014/154557, 2014.

41 C. C. Katsidis and D. I. Siapkas, *Appl. Opt.*, 2002, **41**, 3978–3987.

42 M. C. Troparevsky, A. S. Sabau, A. R. Lupini and Z. Zhang, *Opt. Express*, 2010, **18**, 24715–24721.

43 M. Bellingeri, A. Chiasera, I. Kriegel and F. Scotognella, *Opt. Mater.*, 2017, **72**, 403–421.

44 D. Comoretto, C. Cuniberti, G. F. Musso, G. Dellepiane, F. Speroni, C. Botta and S. Luzzati, *Phys. Rev. B: Condens. Matter Mater. Phys.*, 1994, **49**, 8059–8066.

45 L. Berti, M. Cucini, F. Di Stasio, D. Comoretto, M. Galli, F. Marabelli, N. Manfredi, C. Marinzi and A. Abbotto, *J. Phys. Chem. C*, 2010, **114**, 2403–2413.

46 S. Nam, N. Oh, Y. Zhai and M. Shim, *ACS Nano*, 2015, **9**, 878–885.

47 C. Xiang, W. Koo, F. So, H. Sasabe and J. Kido, *Light: Sci. Appl.*, 2013, **2**, e74.

48 K. Wang, S. Wang, S. Xiao and Q. Song, *Adv. Opt. Mater.*, 2018, **6**, 1800278.